transferred into a Teflon-lined autoclave and heated at 130 °C for 24 h. Glycerol was used as the medium for crystallization because due to the low solubility of silica in this medium, the framework was better retained during crystallization. Finally the solid product was filtered, washed with distilled water, dried at 80 °C, and calcined at 550 °C.

*Characterization*: Nitrogen adsorption/desorption isotherms at −196 °C were established by using an Omnisorp-100 apparatus. The specific surface area, $S_{BET}$, was determined from the linear part of the BET equation ($P/P_0 = 0.05 - 0.15$). The mesopore size distribution was calculated by using the desorption branch of the $N_2$ adsorption/desorption isotherms and the BJH formula. The mesopore surface area $S_{BJH}$ and the mesopore volume $V_{BJH}$ were obtained from the pore size distribution curves. The average mesopore diameter, $D_{BJH}$, was calculated as $4V_{BJH}/S_{BJH}$. Although its accuracy is limited, the BJH method, which is still universally utilized in the literature on mesoporous molecular sieves, yields results that may easily be compared with the current literature. High-resolution TEM images were obtained on a JEOL 200 CX transmission electron microscope operated at 120 kV. The samples for the TEM images were prepared by dispersing the fine powders of the products through a slurry in ethanol onto holey carbon copper grids. Solid-state $^{27}Al$ and $^{29}Si$ MAS NMR spectra were recorded at room temperature using a Bruker ASX 300 spectrometer.

Received: October 11, 2001 [Z18045]


[1] a) C. T. Kresge, M. E. Leonowicz, W. J. Roth, J. C. Vartuli, J. S. Beck, *Nature* **1992**, *359*, 710 – 712.

[2] a) D. Zhao, J. Feng, Q. Huo, N. Melosh, G. H. Fredrickson, B. F. Chmelka, G. D. Stucky, *Science* **1998**, *279*, 548 – 552; b) P. Yang, D. Zhao, D. I. Margolese, B. F. Chmelka, G. D. Stucky, *Nature* **1998**, *396*, 152.

[3] P. Schmidt-Winkel, W. W. Lukens, Jr., D. Zhao, P. Yang, B. F. Chmelka, G. D. Stucky, *J. Am. Chem. Soc.* **1999**, *121*, 254 – 255; P. Schmidt-Winkel, W. W. Lukens, J. P. Yang, D. I. Margolese, J. S. Lettow, J. Y. Ying, G. D. Stucky, *Chem. Mater.* **2000**, *12*, 686.

[4] D. Trong On, D. Giscard, C. Danumah, S. Kaliaguine, *Appl. Catal. A* **2001**, *222*, 299 – 357.

[5] A. Corma, *Chem. Rev.* **1997**, *97*, 2373.

[6] a) D. Trong On, P. N. Joshi, S. Kaliaguine, *J. Phys. Chem.* **1996**, *100*, 6743; b) E. Dumitriu, D. Trong On, S. Kaliaguine, *J. Catal.* **1997**, *170*, 150.

[7] a) D. Trong On, S. M. J. Zaidi, S. Kaliaguine, *Microporous Mesoporous Mater.* **1998**, *22*, 211; b) D. Trong On, M. P. Kapoor, P. N. Joshi, L. Bonneviot, S. Kaliaguine, *Catal. Lett.* **1997**, *44*, 171.

[8] A. Karlsson, M. Stocker, R. Schmidt, *Microporous Mesoporous Mater.* **1999**, *27*, 181.

[9] L. Huang, W. Guo, P. Deng, Z. Xue, Q. Li, *J. Phys. Chem. B* **2000**, *104*, 2817.

[10] a) Y. Liu, W. Zhang, T. J. Pinnavaia, *J. Am. Chem. Soc.* **2000**, *122*, 8791; b) Y. Liu, W. Zhang, T. J. Pinnavaia, *Angew. Chem.* **2001**, *113*, 1295; *Angew. Chem. Int. Ed.* **2001**, *40*, 1255.

[11] Z. Zhang, Y. Han, L. Zhu, R. Wang, Y. Yu, S. Qiu, D. Zhao, F.-S. Xiao, *Angew. Chem.* **2001**, *113*, 1298; *Angew. Chem. Int. Ed.* **2001**, *40*, 1258.

[12] a) D. Trong On, S. Kaliaguine, *Angew. Chem.* **2001**, *113*, 3348; *Angew. Chem. Int. Ed.* **2001**, *40*, 3248; b) D. Trong On, D. Lutic, S. Kaliaguine, *Microporous Mesoporous Mater.* **2001**, *44*, 435.

[13] a) C. E. A. Kirschhock, V. Buschmann, S. Kremer, R. Ravishankar, C. J. Y. Houssin, B. L. Mojet, R. A. van Santen, P. J. Grobet, P. A. Jacobs, J. A. Martens, *Angew. Chem.* **2001**, *113*, 2707; *Angew. Chem. Int. Ed.* **2001**, *40*, 2637; b) P. P. E. A. de Moor, T. P. M. Beelen, R. A. van Santen, L. W. Beck, M. E. Davis, *J. Phys. Chem. B* **2000**, *104*, 7600.

[14] P. P. E. A. de Moor, T. P. M. Beelen, B. U. Komanschek, L. W. Beck, P. Wagner, M. E. Davis, R. A. van Santen, *Chem. Eur. J.* **1999**, *5*, 2083.

[15] Z. Luan, C.-F. Cheng, W. Zhou, J. Klinowski, *J. Phys. Chem.* **1995**, *99*, 1019.


## Diffusion-Limited, Aggregation-Based, Mesoscopic Assembly of Roughened Core – Shell Bimetallic Nanoparticles into Fractal Networks at the Air – Water Interface**

Yongdong Jin and Shaojun Dong*

The collective electronic, optical, and magnetic properties of organized assemblies of size-monodisperse nanocrystals are increasingly the subjects of investigation.[1] Control over the spatial arrangement of these building blocks often leads to new materials with chemical, mechanical, optical, or electronic properties distinctly different from those of their component parts.[2] Recently, metallic fractal clusters have sparked much interest because the localization of dynamical excitations in these fractal objects is a universal property which plays important roles in many physical processes.[3] In particular, the localization of resonant dipolar eigenmodes can lead to a dramatic enhancement of many optical effects in fractals.[3] For example, strongly fluctuating local fields in metallic fractal clusters can significantly exceed the external field and brings about a large enhancement of Raman scattering from the fractals.[4] Highly localized, laser-excited optical modes of silver colloid fractal clusters have been observed by photon scanning tunneling microscopy, and the results verify the main concepts of the resonant optical theory developed for fractal objects.[3] The localization of optical excitations and selective photomodification were also studied experimentally in fractal aggregates of silver colloidal nanoparticles.[5] These results prelude promising interesting applications, especially towards future nano-optics.[5, 6] Therefore, the synthesis of metallic fractal clusters is worthwhile for more detailed theoretical and technological studies.

In contrast to the wealth of recent theoretical work, experimental studies that can test the validity and applicability of modern theories have been rather sparse. In those studies performed, metallic fractal clusters were prepared from spherical colloidal particles by the addition of an adsorbate as a promoter (such as phthalazine,[3, 7] pyridine,[8] or gelatin,[5]) to the solution. Strictly speaking, these aggregates are three-dimensional in solution. However, they collapse upon drying to form nearly flat, two-dimensional (2D) structures. Indeed, it is quite likely that deposition and evaporation of the colloid onto the grid lead to additional aggregation. Herein, we report on a genuine aggregation-based strategy to prepare mesoscopic, two-dimensional fractal aggregates (even thin films) of bare (without adsorbate) silver/gold roughened core – shell nanoparticles by diffusion-limited aggregation (DLA) at the air – water interface by

[*] Prof. S. Dong, Dr. Y. Jin
State Key Laboratory of Electroanalytical Chemistry
Changchun Institute of Applied Chemistry
Chinese Academy of Sciences
Changchun 130022, Jilin (P.R. China)
Fax: (+86) 0431-5689711
E-mail: dongsj@ns.ciac.jl.cn.

[**] We gratefully acknowledge the National Natural Science Foundation of China (Grant Nos. 29835120, 29875028, 20075028) for support of this research and thank Prof. E. K. Wang for helpful discussions and generous support.

  1433-7851/02/4106-1040 $ 17.50+.50/0 

thermoaccelerated electroless plating. We also demonstrate that control over the concentration of the plating solution can not only be used to fine-tune the resulting fractal patterns, but can also drastically affect the crystal growth of the particles.

The Ag nanoparticles prepared by trisodium citrate reduction of $AgNO_3$[9] generate faceted particles with a diameter of about 50 nm, as confirmed by transmission electron microscopy (TEM, Figure 1 A). We used those preformed Ag nanoparticles as seeds to prepare colloidal silver/gold core–shell bimetallic nanoparticles by electroless plating[10, 11] and

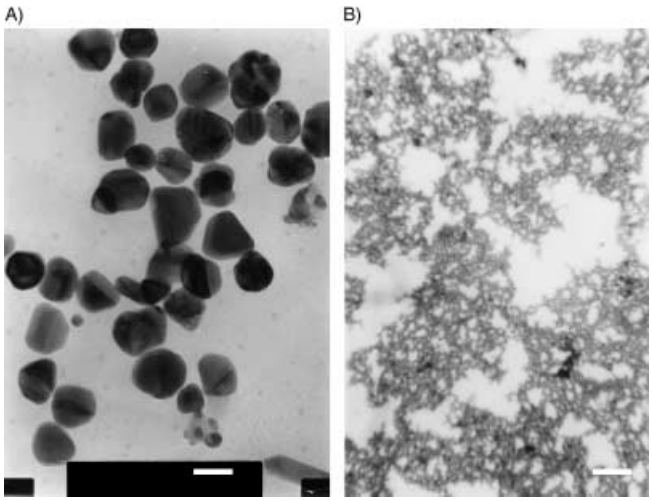


Figure 1. A) TEM image of trisodium citrate prepared Ag nanoparticles showing the size and facet of particles; scale bar = 50 nm. B) Optical microscope image of as-prepared mesoscopic fractal aggregates of Ag/Au core–shell composite nanoparticles. Note the resemblance of the dendritic outline to the modeled results of DLA of metal particles;[12, 13] scale bar = 0.1 mm.

demonstrated that the shapes of the resulting particles could be conveniently varied from a nearly spherical morphology to a roughened one by controling the plating temperature. We also found that the heating time is crucial for preparing roughened colloidal particles. Overheating causes the resulting roughened colloidal particles to float up and be liberated at the air–water interface, a process which results in the formation of fractal aggregates. In the preparation of sample 1, the solution obtained on addition of plating solution ($HAuCl_4$/$NH_2OH$) exhibited a dramatic color change from greenish yellow, which is typical for uncoated Ag sols, to blue. After boiling the solution for about 5 min, some small black dots emerged which could be seen at the air–water interface by the naked eye. The dots grew quickly and exhibited fractal-like patterns on the millimeter to centimeter scale within a few minutes. No precipitate formed during the procedure. The optical photograph of these fractal aggregates (Figure 1 B) shows they are open-structured and in good agreement with the modeled results of diffusion-limited aggregation of metal particles.[12, 13] The composite nanoparticle aggregates exhibit unique collective optical properties, such as being blue colored with a gold reflectance, which are indicative of the existence of hundreds and thousands of linked Au-coated Ag nanoparticles.

We further investigated the fine structures of the fractal aggregates directly by TEM. To our surprise the nanoparticles slightly agglutinate to yield networks (Figure 2 A) and link

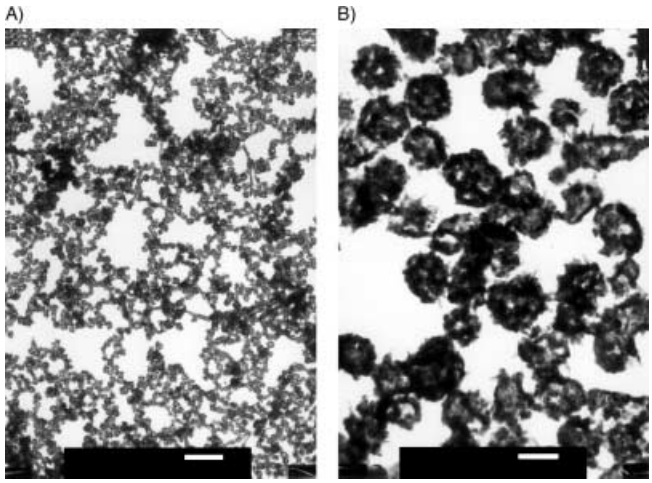


Figure 2. A) TEM image of sample 1 showing the fractal network of linked and still well-dispersed nanoparticles; scale bar = 500 nm. B) A high magnification TEM image of (A). Note the core–shell structure and roughened morphology of the nanoparticles. These composite nanoparticles stick together through the whiskers of particles; scale bar = 100 nm.

together through "junctions" to form a well-defined, two-dimensional porous structure. Aggregation does not produce coalescence into larger particles, but instead produces assemblies of nanoparticle monomers. No three-dimensional aggregation occurs. The morphology is characterized by their tenuous, chainlike structure, and is scale invariant, that is, fractal.[8, 13] An enlarged TEM image clearly showed that the composite nanoparticles are still well dispersed and consist of very uniform diameter crystalline cores (typically about 50 nm in diameter) surrounded by a heterogeneous roughened (whiskerlike) coating (Figure 2 B). Indeed, the core–shell nanoparticles stick together through the whiskers of the particles. No whisker growth was evident in a control experiment without heating. This result suggests that there is a thermo-induced preferential direction of growth of Au on the facets of Ag nanoparticles. This growth of the whiskers occurs as a result of differences in the curvature-dependent local chemical potentials.[14]. We elucidated the composition of the core and whiskerlike shell by using X-ray photoelectron spectra (XPS) analysis of self-assembled monolayers on glass slides modified with 3-aminopropyltrimethoxysilane (APTMS) before and after electroless Au plating (Figure 3). These experiments, in combination with TEM image analysis,[11] revealed that the prepared Ag/Au nanoparticles had a core–shell structure, and confirmed that the particles consist of an Ag core and an Au shell enriched with Ag.[11]

The fractal patterns of the nanocrystal aggregates can be fine-tuned by changing the concentration of the plating solution. At low $HAuCl_4$ concentrations (sample 2) there are more open spaces in the well-ramified pattern and whisker-linked nanoparticles align almost one-by-one (Figure 4 A). More interestingly we also observed a seed particle

  1433-7851/02/4106-1041 $ 17.50+.50/0 

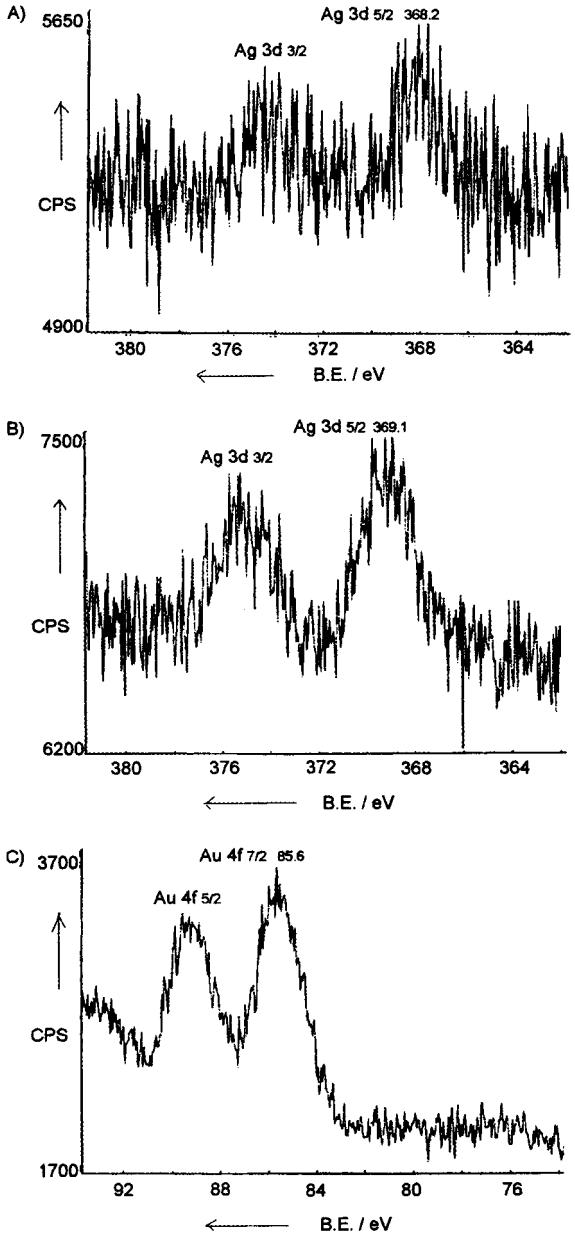


Figure 3. XPS (ESCLAB MKII, using Mg as the exciting source) analysis of Ag 3d orbitals of the Ag nanoparticles prepared by trisodium citrate reduction (A), the Ag 3d orbitals (B), and Au 4f orbitals (C) of as-prepared Ag/Au core–shell roughened nanoparticles. B.E. = binding energy, CPS = counts per second.

(blackest dot in Figure 4B) in the selected image area, which is typically characteristic of a DLA model.[12] At higher $HAuCl_4$ concentrations (sample 3) the particles are linked relatively compactly and there are less crevices in the networks (Figure 5A), which fit better to the Eden model[12, 13]—a lattice model in which particles are added one at a time to random sites adjacent to occupied sites. The TEM images show that increasing the concentration of $HAuCl_4$ changes the fractal patterns of the resulting aggregates from a DLA model to an Eden-like model. It is also noteworthy that the as-prepared 2D fractal aggregates are robust and flexible, which can be confirmed by the presence of some small particle loops in the TEM images.

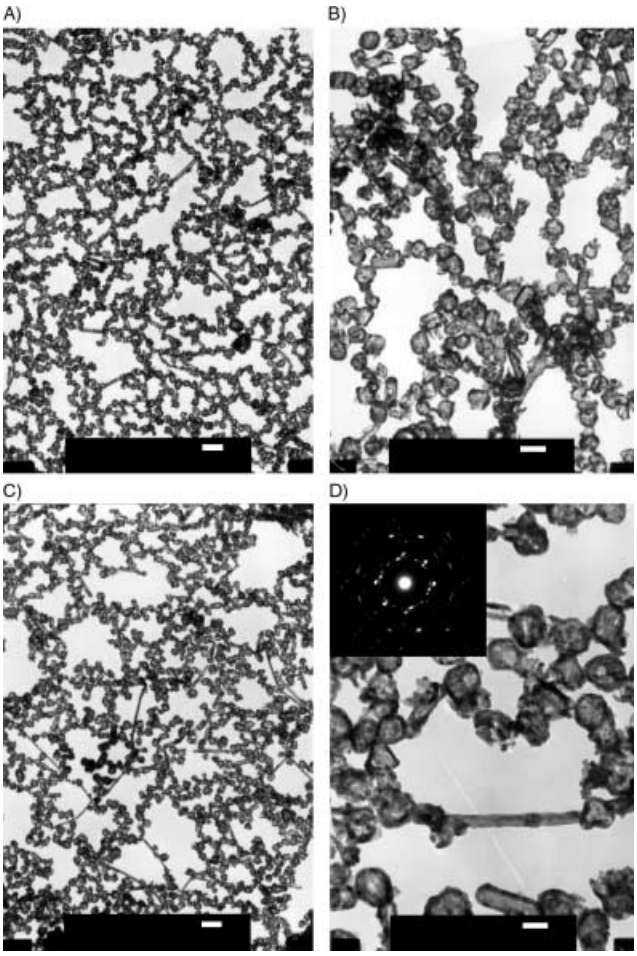


Figure 4. A) A typical TEM image of sample 2. The composite particles aligned almost one-by-one and well ramified; scale bar = 200 nm. B) A high-magnification TEM image of (A) showing a seed particle (black dot) in the selected area and its following DLA growth traces; scale bar = 100 nm. C) Another typical TEM image of sample 2, which explicitly shows the presence of some nanorods and nanowires; scale bar = 200 nm. D) A high-magnification TEM image of a resulting nanowire and the corresponding electron diffraction pattern (inset); scale bar = 50 nm.

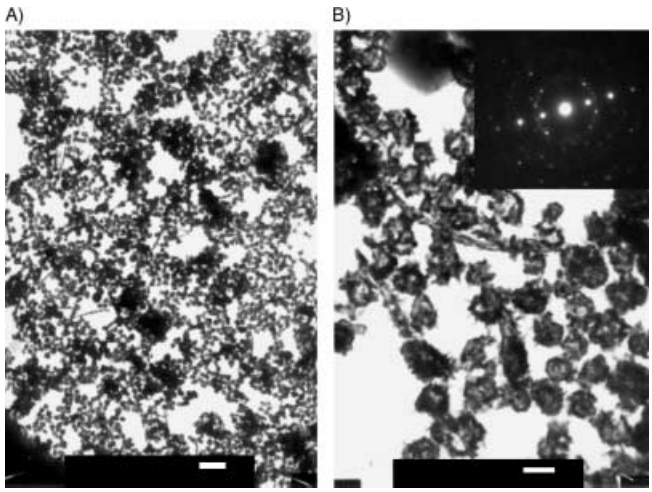


Figure 5. A) A typical TEM image of sample 3 showing the size and shape distribution of single crystals growing in a nanoconfined environment among the relatively compact particle network; scale bar = 500 nm. B) A high-magnification TEM image of a resulting single crystal in (B) and the corresponding electron diffraction pattern (inset); scale bar = 100 nm.

  1433-7851/02/4106-1042 $ 17.50+.50/0 

The TEM images also showed that a variation of the $HAuCl_4$ concentration affects the crystal growth of the particles, as well as changing the fractal pattern of resulting aggregates. When the $HAuCl_4$ concentration is increased, the shell thickness increases and the whiskers grow faster and longer. Interestingly, many large, square and triangular single crystals begin to grow and scatter evenly among the networks, as evident in Figure 5A and confirmed by the corresponding electron diffraction pattern (Figure 5B). We were able to determine the three-dimensional shapes of the particles by tilting the samples in the TEM experiment. The particles with square outlines were found to be cubic, while those with triangular outlines were tetrahedral. No large single crystals grow in the nanoconfined environment at low $HAuCl_4$ concentrations, but many nanorods and nanowires grow instead. Figure 4C shows a typical image of the resulting nanorods and nanowires. It clearly shows that the remarkably uniform diameters of the nanowires are on the order of about 50 nm (dictated almost by the diameter of the Ag particles) and the length is on the order of about 0.5–1 μm. Furthermore, the highly crystalline nature of the resulting nanowires was confirmed by selected-area electron diffraction measurements on these nanowires (Figure 4D). The diffraction spots/rings reveal a hexagonal diffraction spot pattern, which indicates that the Au nanowires prepared by surface catalysis of the Ag nanoparticles are almost single crystals growing along the [111] direction. Incidentally, the growth behavior of the resulting nanowires is very similar to that seen in the catalytic synthesis of nanowires by laser ablation.[15]

An experimental model to shed further light on the growth process of these fractal aggregates is shown in Figure 6. When the reaction solution is heated, thermo-induced selective growth of Au on the surface of Ag nanoparticles results in the rapid growth of whiskers. When the whiskers have grown long enough, the resulting global dendrites float up and are liberated at the air–water interface as "random walkers".[13] They wander freely and quickly until they collide and irreversibly stick together,[16] by a subsequent deposition step, to become part of the cluster. The initial liberated particle acts as a seed particle during this cluster aggregation. The exposed ends of the clusters grow more rapidly than the interior since the "random walkers" are captured before they reach the interior. Thus, the resulting cluster has a tenuous treelike and open structure because holes are formed and not filled up.[13] Following cluster aggregation, the cluster–cluster aggregation proceeds[13] to produce more open and fluffy structures. As a result, the aggregates grow and finally reach millimeter to centimeter scales at the air–water interface.

It is well known that DLA is an idealization of the process by which matter irreversibly combines to form dust, soot, dendrites, and other random objects when the rate-limiting step is the diffusion of matter to the aggregate. The growth of a DLA cluster is determined by the set of growth probabilities $\{P_i\}$, where $P_i$ is the next unit to be added to the cluster.[17] The simplicity of the experiments described here represents a good experiment model and is of fundamental and technological interest to gain insight into the nature of DLA and controlled fractal growth.

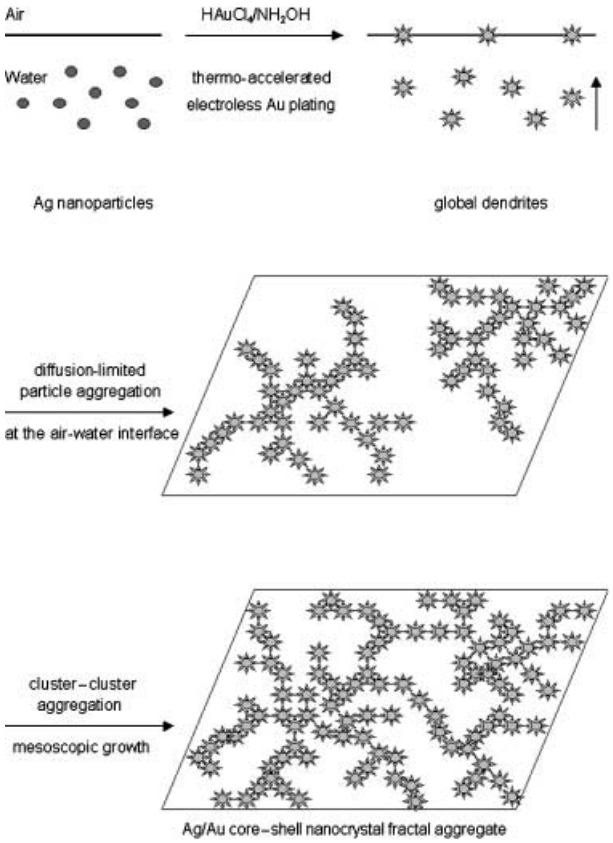


Figure 6. Schematic representation of the growth and assembly process of silver/gold roughened core-shell nanoparticles into mesoscopic fractal networks at the air-water interface.

It is important to note that the as-prepared fractal aggregates consist of hundreds and thousands of structurally well-defined Ag/Au core–shell nanoparticles, which may exhibit unique mesoscopic electrical and optical properties[3–6] that depend sensitively on both the size and fractal dimensionality. The method described here should be useful, not only for testing theories of fractal growth, but also for enriching synthetic methods of nanomaterials with controlled properties. Importantly, the ease of solution-phase synthesis in combination with the ability to control the long-range assembly of the composite nanoparticles into continuous fractal-defined structures make this artificial "macromolecules" architecture—silver nanoparticles (artificial atoms) linked together by nanoscale gold whiskers (bonds)—a further step toward artificial solids made of large arrays of linked dots.[18] Very recently, we have also found, by mild modification of the method described herein, that the fractal aggregates can gradually grow and finally fill the whole surface of the container used, thus proving that it is possible to scale-up this technology for the facile preparation of quasi-two dimensional, structurally well-defined porous fractal thin films of composite roughened nanoparticles with controlled sizes. This possibility will hold great promise for potential fundamental and technological applications.[3–6, 18]

*Experimental Section*

Analytical grade $HAuCl_4 \cdot 3H_2O$, trisodium citrate, hydroxylamine hydrochloride, and $AgNO_3$ were all obtained from Aldrich and used without

further purification. All glassware used in the following procedures were cleaned in a bath of freshly prepared 3:1 HCl:$HNO_3$ (aqua regia) and rinsed thoroughly in milli-Q grade water prior to use. The Ag nanoparticles were prepared by sodium citrate reduction of $AgNO_3$:[9] $AgNO_3$ (18 mg) was dissolved in $H_2O$ (100 mL) and brought to reflux. A solution of 1% trisodium citrate (2 ml) was added and the solution was kept at reflux for about 1 h. The final volume was adjusted to 500 mL. The Ag sols prepared were greenish yellow. The Ag plasmon absorbance maxima was at approximately 440 nm.

In a typical synthesis, as-prepared Ag sols (5 mL) was diluted with water (5 mL), then a freshly prepared plating solution of 0.02 M $NH_2OH$ (0.10 mL) and 0.1% $HAuCl_4$ (0.25 mL) was added with stirring. The solution was then heated at reflux for about 10 min before cooling it down to room temperature. It was now ready for TEM sample preparation (sample 1). Samples 2 and 3 were prepared by adding 0.10 and 1.0 mL of a 0.1% solution of $HAuCl_4$ to the aliquot Ag sols, respectively, and then following the same procedure as for sample 1. The initial ratios of the concentration of the $HAuCl_4$ solution were 2.5:1:10 for samples 1, 2, and 3, respectively.

Samples for TEM were prepared by placing a drop of solution (for sol) on or transferring as-prepared thin film to a carbon-coated copper grid. Samples were examined by using a JEOL 2010 transmission electron microscopy operated at 200 kV. Analysis of the X-ray photoelectron spectra (XPS) was performed on a ESCLAB MKII using Mg as the exciting source.

Received: September 26, 2001
Revised: January 8, 2002 [Z17973]

[1] a) A. P. Alivisatos, *Science* **1996**, *271*, 933 – 937, and references therein; b) R. P. Andres, J. D. Bielefeld, J. I. Henderson, D. B. Janes, V. R. Kolagunta, C. P. Kubiak, W. J. Mahoney, R. G. Osifchin, *Science* **1996**, *273*, 1690 – 1693; c) C. B. Murray, C. R. Kagan, M. G. Bawendi, *Science* **1995**, *270*, 1335 – 1338; d) D. Ryan, S. N. Rao, H. Rensmo, D. Fitzmaurice, J. A. Preece, S. Wenger, J. F. Stoddart, N. Zaccheroni, *J. Am. Chem. Soc.* **2000**, *122*, 6252 – 6257.
[2] a) S. M. Marinakos, S. M. D. A. Schultz, D. L. Feldheim, *Adv. Mater.* **1999**, *11*, 34 – 37, and references therein; b) A. N. Shipway, E. Katz, I. Willner, *ChemPhysChem* **2000**, *1*, 18 – 52.
[3] D. P. Tsai, J. Kovacs, Z. H. Wang, M. Moskovits, V. M. Shalaev, J. S. Suh, R. Botet, *Phys. Rev. Lett.* **1994**, *72*, 4149 – 4152, and references therein.
[4] a) V. M. Shalaev, M. I. Stockman, *Zh. Eksp. Teor. Fiz.* **1987**, *92*, 509 (*Soviet Physics-JETP* **1987**, *65*, 287); b) V. M. Shalaev, M. I. Stockman, *Z. Phys. D* **1988**, *10*, 71; c) M. I. Stockman, V. M. Shalaev, M. Moskovits, R. Botet, T. F. George, *Phys. Rev. B* **1992**, *46*, 2821 – 2830.
[5] V. P. Safonov, V. M. Shalaev, V. A. Markel, Yu. E. Danilova, N. N. Lepeshkin, W. Kim, S. G. Rautian, R. L. Armstrong, *Phys. Rev. Lett.* **1998**, *80*, 1102 – 1105.
[6] a) M. Quinten, A. Leitner, J. R. Krenn, F. R. Aussenegg, *Opt. Lett.* **1998**, *23*, 1331 – 1333; b) J. R. Krenn, A. Dereux, J. C. Weeber, E. Bourillot, Y. Lacroute, J. P. Goudonnet, G. Schider, W. Gotschy, A. Leitner, F. R. Aussenegg, C. Girard, *Phys. Rev. Lett.* **1999**, *82*, 2590 – 2593.
[7] M. Moskovits, J. S. Suh, *J. Phys. Chem.* **1984**, *88*, 5526 – 5530.
[8] a) D. A. Weitz, M. Oliveria, *Phys. Rev. Lett.* **1984**, *52*, 1433 – 1436; b) N. Félidj, G. Lévi, J. Pantigny, J. Aubard, *New J. Chem.* **1998**, 725 – 732.
[9] P. C. Lee, D. Melsel, *J. Phys. Chem.* **1982**, *86*, 3391 – 3395.
[10] K. R. Brown, M. J. Natan, *Langmuir* **1998**, *14*, 726 – 728.
[11] I. Srnová-Šloufová, F. Lednický, A. Gemperle, J. Gemperlová, *Langmuir* **2000**, *16*, 9928 – 9935.
[12] T. A. Witten, L. M. Sander, Jr., *Phys. Rev. Lett.* **1981**, *47*, 1400 – 1403.
[13] L. M. Sander, *Nature* **1986**, *322*, 789 – 793.
[14] N. Combe, P. Jensen, A. Pimpinelli, *Phys. Rev. Lett.* **2000**, *85*, 110 – 113.
[15] A. M. Morales, C. M. Lieber, *Science* **1998**, *279*, 208 – 211.
[16] S. Meltzer, R. Resch, B. E. Koel, M. E. Thompson, A. Madhukar, A. A. G. Requicha, P. Will, *Langmuir* **2001**, *17*, 1713 – 1718.
[17] J. Lee, H. E. Stanley, *Phys. Rev. Lett.* **1988**, *61*, 2945 – 2948.
[18] R. C. Ashoori, *Nature* **1996**, *379*, 413 – 419, and references therein.

# The First Water-Soluble Copper(I) Calix[6]arene Complex Presenting a Hydrophobic Ligand Binding Pocket: A Remarkable Model for Active Sites in Metalloenzymes**

Yannick Rondelez, Gildas Bertho, and Olivia Reinaud*

Because of the unique properties of water, the synthesis of biomimetic complexes that are soluble and stable under physiological conditions is an attractive goal. Paradoxically, most metalloenzyme models have been developed in organic solvents.[1] The first reason is that the ligands used to mimic the biological active site often lead to water-insoluble complexes, and their solubilization through synthetic procedures is not an easy task. For instance, tris(pyrazolyl)borate, which is the basis for countless biomimetic complexes,[2] is sensitive to hydrolysis, and hydrophilic derivatives would not survive in aqueous solvent.[3] The second reason is that biologically relevant species are often reactive to water and must be protected and/or stabilized. In the specific case of copper, few water-soluble cuprous complexes have been described,[3, 4] and to the best of our knowledge none of them can be considered biomimetic. Indeed, it is well known that $Cu^I$ centers are thermodynamically unstable in water and disproportionate in the absence of an appropriate coordinating environment. Another major difficulty stems from the fact that metalloenzyme model complexes must present a vacant or a labile site on the metal center to allow the coordination and/or activation of a guest.

In the course of modeling type 2 active sites of copper enzymes, we have been interested in developing a supramolecular system that can stabilize a copper(I) center within a biomimetic environment.[5–7] We have now extended our previous work to demonstrate a possible route to transform the calix[6]arene derivatives soluble in organic solvents into compounds soluble in water. Here, we describe the synthesis of the first water-soluble biomimetic cuprous complex.

The selectively functionalized calix[6]arene derivative **1**[8] was first *O*-alkylated with three imidazole arms to yield compound **2** (Scheme 1).[6] The next step consisted of the *ipso* sulfonation of the three anisole rings by treating **2** with concentrated sulfuric acid. The resulting triacid **[3]** · $H_3$ was neutralized with sodium hydroxide, giving rise to the trisodium salt **[3]** · $Na_3$. This new ligand is highly soluble in water and, to a lesser extent, in methanol, ethanol, and 2-propanol.

[*] Dr. O. Reinaud, Y. Rondelez, G. Bertho
Laboratoire de Chimie et Biochimie Pharmacologiques et Toxicologiques
CNRS UMR 8601, Université René Descartes
45 rue des Saints-Pères, 75270 Paris Cedex 06 (France)
Fax: (+33) 1-42-86-83-87
E-mail: reinaud@biomedicale.univ-paris5.fr

[**] We would like to thank Dr. Michèle Salmain (ENSCP, Paris) for her help with the IR spectroscopy experiments performed in water, and express our gratitude to Dr. Olivier Laprevotte (ICSN, Gif-sur-Yvette) for electron spray mass spectra.

Supporting information for this article is available on the WWW under http://www.angewandte.com or from the author.

  1433-7851/02/4106-1044 $ 17.50+.50/0 